Reaching for the stars – JWST/NIRSpec spectroscopy of a lensed star candidate at $z = 4.76$

Lukas J. Furtak [ORCID],[1]★ Ashish K. Meena [ORCID],[1] Erik Zackrisson [ORCID],[2] Adi Zitrin [ORCID],[1] Gabriel B. Brammer,[3] Dan Coe,[4,5,6] José M. Diego [ORCID],[7] Jan J. Eldridge [ORCID],[8] Yolanda Jiménez-Teja,[9,10] Vasily Kokorev,[11] Massimo Ricotti,[12] Brian Welch,[12,13] Rogier A. Windhorst,[14] Abdurro'uf,[4,6] Felipe Andrade-Santos,[15,16] Rachana Bhatawdekar,[17] Larry D. Bradley,[4] Tom Broadhurst,[18,19,20] Wenlei Chen,[21] Christopher J. Conselice,[22] Pratika Dayal [ORCID],[11] Brenda L. Frye,[23] Seiji Fujimoto [ORCID],[24] Tiger Y.-Y. Hsiao [ORCID],[6] Patrick L. Kelly,[20] Guillaume Mahler [ORCID],[25,26] Nir Mandelker [ORCID],[27] Colin Norman,[4,6] Masamune Oguri,[28,29] Norbert Pirzkal,[4] Marc Postman,[4] Swara Ravindranath,[4] Eros Vanzella[30] and Stephen M. Wilkins [ORCID][31,32]

Affiliations are listed at the end of the paper

ABSTRACT

We present JWST/NIRSpec observations of a highly magnified star candidate at a photometric redshift of $z_{phot} \simeq 4.8$, previously detected in JWST/NIRCam imaging of the strong lensing (SL) cluster MACS J0647+7015 ($z = 0.591$). The spectroscopic observation allows us to precisely measure the redshift of the host arc at $z_{spec} = 4.758 \pm 0.004$, and the star's spectrum displays clear Lyman- and Balmer-breaks commensurate with this redshift. A fit to the spectrum suggests a B-type super-giant star of surface temperature $T_{eff,B} \simeq 15\,000$ K with either a redder F-type companion ($T_{eff,F} \simeq 6\,250$ K) or significant dust attenuation ($A_V \simeq 0.82$) along the line of sight. We also investigate the possibility that this object is a magnified young globular cluster rather than a single star. We show that the spectrum is in principle consistent with a star cluster, which could also accommodate the lack of flux variability between the two epochs. However, the lack of a counter image and the strong upper limit on the size of the object from lensing symmetry, $r \lesssim 0.5$ pc, could indicate that this scenario is somewhat less likely – albeit not completely ruled out by the current data. The presented spectrum seen at a time when the Universe was only ~ 1.2 Gyr old showcases the ability of JWST to study early stars through extreme lensing.

Key words: gravitational lensing: micro – gravitational lensing: strong – stars: individual: MACS0647-star-1 – stars: massive – galaxies: high-redshift – galaxies: star clusters: general.

1 INTRODUCTION

One of the main goals of JWST (Gardner et al. 2023), launched in 2021 December, is to detect the very first stars and galaxies that populated the universe. Directly observing individual stars at large extragalactic or cosmological distances is however not possible, since they would simply be too dim. Nonetheless, in the past few years several stars at cosmological distances have been detected at various redshifts, thanks to the gravitational lensing effect: individual stars in lensed background galaxies can become sufficiently magnified to be detected as they near a lensing-cluster's caustic (Miralda-Escude 1991).

The first example of such a lensed star is *Icarus* at $z \simeq 1.49$ (Kelly et al. 2018), which was detected in the field of the galaxy cluster MACS J1149.5+2223 as a transient event roughly atop the expected position of the critical curve, where the magnification is extremely high. A spectral energy distribution (SED) fit to the star's photometry yielded constraints on its spectral type and surface temperature (a B-type super-giant with $T_{eff} \simeq 11\,000 - 14\,000$ K; Kelly et al. 2018).

Since then, several dozen other such lensed stars at cosmological distances have been detected in various strong lensing (SL) cluster fields, both serendipitously (e.g. Chen et al. 2019; Kaurov et al. 2019) or in designated surveys (e.g. the *Flashlights* survey; Kelly et al. 2022; Diego et al. 2023a; Meena et al. 2023a). Several were also already detected in JWST imaging campaigns during the first year of the observatory's operations (e.g. Chen et al. 2022; Diego et al. 2023b; Meena et al. 2023b; Diego et al. 2023c). However, not all lensed stars necessarily appear as transient sources. Since the lens is itself made-up of small point or near-point masses such as stars, globular clusters, or black holes, a corrugated web of (micro-) caustics is formed in the source plane in the very high magnification regime around the macro-caustic. If a source star lies in this corrugated network, it can remain extremely magnified for long periods of time (e.g. Venumadhav, Dai & Miralda-Escudé 2017; Diego et al. 2018; Oguri et al. 2018). In general, such caustic networks represent a crucial window of opportunity for studying single stars in detail across the history of the universe since it enables follow-up observations after detection.

Following the redshift distribution of lensed galaxies, most of the known lensed stars have been found at $z \sim 1 - 3$. The currently

farthest known lensed star is *Earendel*, detected with the *Hubble Space Telescope (HST)* at $z \simeq 6.2$ and followed up with JWST imaging (Welch et al. 2022a, b). In Meena et al. (2023b), we recently presented other examples at high redshift: two lensed star candidates were detected near the symmetry point of a giant arc at $z_{\mathrm{phot}} \simeq 4.8$ in the SL cluster MACS J0647.7+7015 (MACS0647; $z = 0.591$; Ebeling et al. 2007). The arc was previously known from *HST* observations of the cluster (e.g. Zitrin et al. 2011; Postman et al. 2012; Coe et al. 2013; Zitrin et al. 2015). The brighter and more reliable of these two lensed star candidates, MACS0647-star-1, had been classified from broad-band photometry in Meena et al. (2023b) to be, most probably, a B-type star with $T_{\mathrm{eff}} \sim 10\,000\,\mathrm{K}$ and $M \gtrsim 20\,\mathrm{M}_{\odot}$. It has now been observed spectroscopically with JWST, delivering an unprecedented spectrum of a lensed star at such a cosmological distance,[1] showcasing JWST's ability to directly probe early stars through extreme lensing.

In this letter, we present the spectrum of MACS0647-star-1, and analyse it to derive the star's properties. This work is organized as follows: in Section 2, we describe the data and observations used in this work. In Section 3 we analyse the spectrum, and the results are discussed in Section 4. The work is concluded in Section 5. Throughout, we assume a standard flat ΛCDM cosmology with $H_0 = 70\,\frac{\mathrm{km}}{\mathrm{s\,Mpc}}$, $\Omega_{\Lambda} = 0.7$, and $\Omega_{\mathrm{m}} = 0.3$. Magnitudes are quoted in the AB system (Oke & Gunn 1983) and uncertainties represent 1σ ranges unless stated otherwise.

2 DATA

The data used in this work were taken with JWST in the framework of GO programme 1433 (PI: D. Coe). The spectrum of MACS0647-star-1 was taken with the *Near-Infrared Spectrograph* (NIRSpec; Jakobsen et al. 2022; Böker et al. 2023) aboard JWST in its multi-object spectroscopy (MOS) mode (Ferruit et al. 2022) using the micro-shutter array (MSA) in standard 3-slitlet nods, to allow local sky subtraction, with a total exposure time of 1.8 h. The slit position and orientation can be seen in Fig. 1. The resulting prism spectrum achieves resolutions of $R \sim 30 - 300$ in the wavelength range from $0.6 - 5.3\,\mu\mathrm{m}$. Additional details regarding the observations, data reduction with the Space Telescope Science Institute (STScI) JWST pipeline,[2] and spectral extraction with MSAEXP[3] are described in detail in Hsiao et al. (2023a).

The imaging data for MACS0647 are comprised of deep *Near-Infrared Camera* (NIRCam; Rieke et al. 2023) observations in 7 filters: F115W, F150W, F200W, F277W, F365W, F444W, and F480M. The F480M imaging and a second epoch of F200W-band exposure were taken at the same time as the NIRSpec observations described earlier. The data were reduced using the grism redshift and line analysis software for space-based spectroscopy pipeline (grizli; Brammer et al. 2022) and achieve exposure times of 35 min band^{-1}. We refer the reader to Hsiao et al. (2023b) and Meena et al. (2023b) for the details regarding the imaging data and their reduction, and the photometric analysis of MACS0647-star-1.
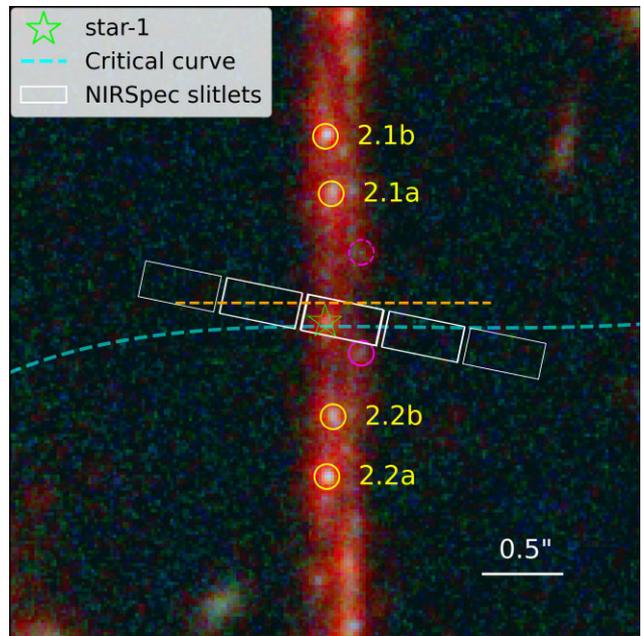
Figure 1. JWST/NIRCam composite-colour image (blue: F115W+F150W, green: F150W+F200W, red: F277W+F356W+F444W) of the $z = 4.758$ caustic-crossing arc in MACS0647 and the lensed stars that it hosts. MACS0647-star-1 is highlighted with a green star and we also show the location of MACS0647-star-2 (magenta solid circle) even though it was not included in the NIRSpec slitlets (white). We also mark a possible counter image for star-2 in dashed purple. The critical curve of the Meena et al. (2023b) SL model of the cluster is overlaid in dashed turquoise and multiply-imaged clumps within the arc are highlighted in yellow. The symmetry line between the multiply-imaged clumps is shown in dashed orange.

3 SPECTROSCOPIC ANALYSIS

The MSA slitlets, shown in Fig. 1, contain both the emission of the star and some diffuse emission from the host galaxy around it. The spectrum, which can be seen in Fig. 2, shows two emission lines that are slightly offset (by 2 pixels) on the spatial axis from the central continuum trace. This means that they originate from a different location than the star, that is, most probably the host galaxy. Together with a prominent Balmer-break observed at $\lambda \sim 2.1\,\mu\mathrm{m}$ and a weaker Lyman-break at $\lambda \sim 0.7\,\mu\mathrm{m}$, we measure the redshift of the host by identifying these two emission lines as the [O III]$\lambda\lambda$4959, 5007 Å-doublet and Hα at $z \simeq 4.8$. There is also a tentative detection of Hβ.[4] The line centres are determined by fitting a Gaussian to each continuum-subtracted emission line with specutils (v1.10.0; Earl et al. 2023) and then estimating the uncertainties with a Monte Carlo Markov Chain (MCMC) analysis using EMCEE (Foreman-Mackey et al. 2013). This yields a spectroscopic redshift measurement of $z_{\mathrm{spec}} = 4.758 \pm 0.004$ for this arc, confirming the photometric redshift of $z_{\mathrm{phot}} = 4.79^{+0.07}_{-0.15}$ from Meena et al. (2023b).

To separate the star candidate's spectrum from contamination by the host arc, we use the fact that the emission lines are spatially offset from the central continuum trace to extract a host galaxy spectrum. This is done by taking a smaller box above the continuum

---

[1] At lower-redshifts, a ground-based spectrum was taken for the lensed star *Godzilla* ($z = 2.37$; Vanzella et al. 2020; Diego et al. 2022) and a JWST/NIRSpec spectrum of *Earendel* is also expected soon (Welch et al. in preparation)

[2] https://github.com/spacetelescope/jwst

[3] https://github.com/gbrammer/msaexp

[4] Assuming a Calzetti et al. (2000) law, this results in a tentative measurement of $A_V = 1.67 \pm 0.33$ for the host galaxy based on the Balmer-decrement (Domínguez et al. 2013). Note that this does not affect our spectral modelling results in Section 4 though since that is only sensitive to very localized dust in the source's immediate surroundings.
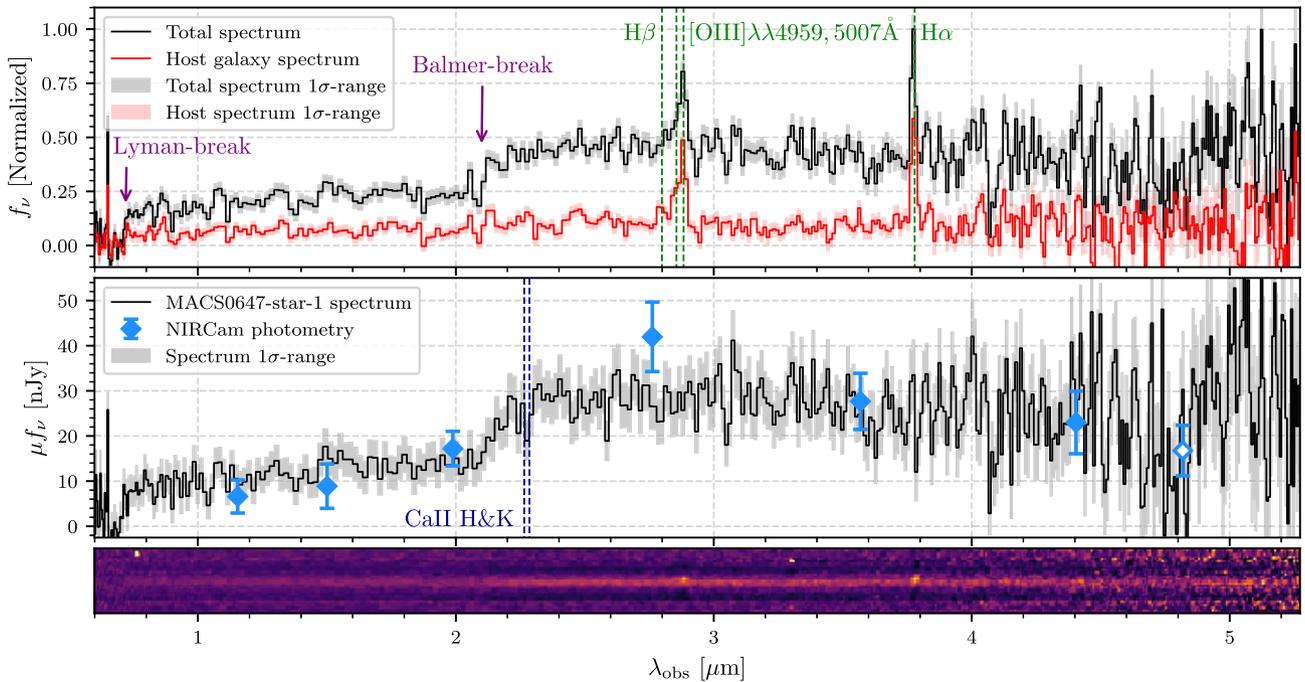
Figure 2. JWST/NIRSpec spectroscopy of MACS0647-star-1. *Bottom*: 2D-spectrum in the JWST/NIRSpec slitlet shown in Fig. 1. The two emission lines are spatially slightly offset from the continuum in the central trace, suggesting they originate from the host galaxy rather than the lensed star itself. *Top*: Total spectrum extracted by MSAEXP (black) and the host galaxy spectrum (red), in arbitrary flux units. The host spectrum is extracted in a smaller box, centred vertically on the offset emission lines' position instead of the continuum. These two prominent emission lines (green) are identified as the (unresolved) [O III]$\lambda\lambda4959$, 5007 Å-doublet and Hα and thus yield a spectroscopic redshift measurement of $z = 4.758 \pm 0.004$. *Middle*: Host-subtracted and flux-calibrated NIRSpec spectrum of MACS0647-star-1 (black) and the corresponding NIRCam photometry (blue squares; the open square represents second-epoch photometry). The spectrum displays clearly visible Lyman- and Balmer-breaks but, as expected given the signal-to-noise, no significant absorption features. That being said, we tentatively observe slight troughs where the Ca II H and K lines (dark blue) can be expected given the redshift. The spectrum as shown here is not corrected for gravitational magnification.

but centred on the emission lines' vertical position, using the same algorithm as the MSAEXP pipeline (see Section 2). The thus obtained 1D-spectrum of the host is then weighted by its contribution to the total trace fit by MSAEXP in the initial data reduction and extraction (see e.g. Hsiao et al. 2023a). As can be seen in the top panel of Fig. 2, the host galaxy spectrum clearly shows the emission lines mentioned earlier and a low level of continuum emission but lacks a strong Balmer-break (red-to-blue flux ratio of 1.6 ± 0.1 measured between the two sides of the break). This host spectrum is then simply subtracted from the total spectrum extracted by MSAEXP to obtain the spectrum of the star. Since the signals of the host and the star are inevitably merged together in the NIRSpec spectrum, a perfect host subtraction can probably not be achieved. This means that we are probably over- or under-subtracting the host contribution. Since the host continuum is fairly flat (see top panel of Fig. 2), we do not expect this to affect the shape of the spectrum though, only its total flux level. Because of that, we renormalize the host-subtracted spectrum to the six bands of broad-band photometry of MACS0647-star-1 measured in Meena et al. (2023b), which also effectively corrects for slit losses. While some fluctuations in magnification can be expected for a persistent lensed star near the caustic (e.g. Jiménez-Vicente & Mediavilla 2022; Welch et al. 2022a), the F200W imaging taken at the same time as the NIRSpec observations (see Section 2) does not show any flux evolution between the two epochs: that is, 28.31 ± 0.24 and 28.27 ± 0.22 magnitudes in the first and second epochs, respectively, measured with CICLE (Jiménez-Teja & Dupke 2016) as in Meena et al. (2023b). We note that given its position, there is a slight possibility that some residue flux from MACS0647-

star-2 (see Fig. 1) entered the slit as well. That contribution would be included in our 'host' spectrum and therefore be subtracted out though.

The thus cleaned and flux-calibrated spectrum of the lensed star is shown in the middle panel of Fig. 2. The host subtraction described above effectively removed the emission lines, indicating a fair subtraction. While the spectrum matches the NIRCam photometry in all bands within the 1σ-range, the Balmer-break seems shallower than that estimated from the photometry in Meena et al. (2023b). While we do not observe any significantly strong absorption features, which is in agreement with the expected signal-to-noise ratio (SNR), the spectrum shows tentative troughs ($\sim 1\sigma$) at the expected wavelengths of the Ca II H and K lines, and more marginally, also near the Fraunhofer G-band, Hγ, and Hβ wavelengths (see also Fig. 3). Given the SNR, however, at this point we should acknowledge that this may simply be coincidental, and that deeper observations will be needed to probe if these are real.

4 SPECTRAL MODELLING

In order to determine the properties of the source, a more quantitative analysis of the spectrum presented in Section 3 is required. We therefore perform detailed spectral modelling, both considering the source to be one, or two individual stars (Section 4.1), or a globular cluster-like object bound to the host galaxy (Section 4.2) and discuss the results in Section 4.3.
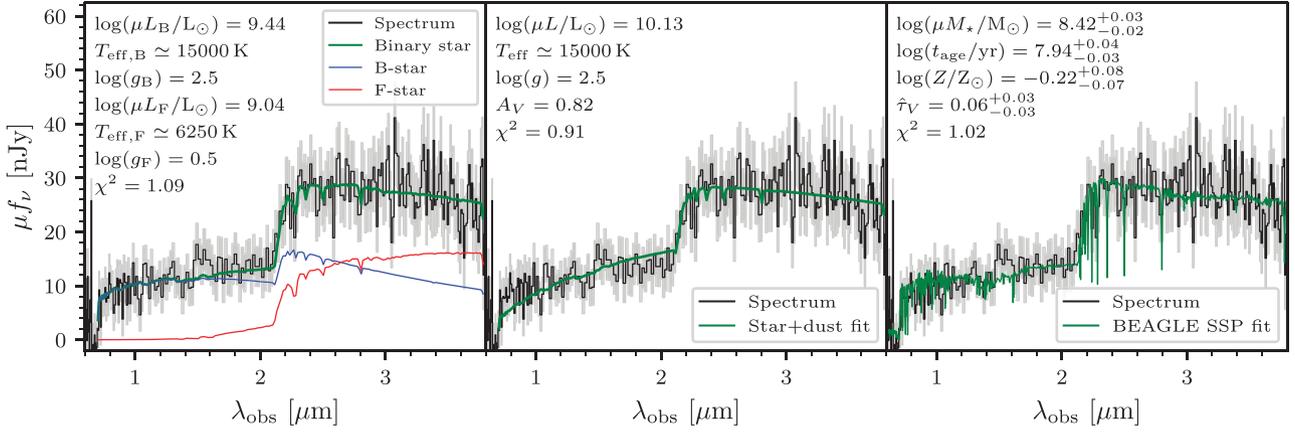
Figure 3. Spectral fits of star and star-cluster templates to the spectrum of MACS0647-star-1, which is shown in black. *Left*: A two-star fit (green). The more luminous component, a B-type star, is shown in blue and the fainter, an F-type star, in red. *Middle*: A single star fit with significant dust attenuation. *Right*: Maximum-a-posteriori (MAP) solution for a globular cluster-type single stellar population (SSP) fit with BayEsian Analysis of GaLaxy sEds (BEAGLE; green).

4.1 Stellar modelling

The Balmer-break of the spectrum is weaker than inferred from the photometry (see Fig. 2), such that the simple single-star solution from Meena et al. (2023b) should be revised here with the spectroscopic data. We therefore attempt to fit the spectrum of MACS0647-star-1 with either a single-star SED with dust attenuation or as a superposition of two single-star SEDs without attenuation. All SED templates are based on the Lejeune, Cuisinier & Buser (1997) set of stellar atmosphere spectra redshifted to $z = 4.76$ and resampled to the observed resolution. At the spectral resolution of the NIRSpec prism, the effect of metallicity is negligible on the shapes of these SEDs, and we therefore only present fits for metallicity [M/H] = -1 (but have verified that [M/H] = 0 does not have any significant impact on our conclusions). Since we are likely dealing with very massive stars, we moreover limit the fits to the lowest surface gravities available at each effective temperature $T_{\rm eff}$ within the grid. For the dust attenuation, we adopt the Calzetti et al. (2000) law, as parametrized by Li et al. (2008).

The resulting best fit SEDs are shown in the left-hand and middle panels of Fig. 3. In the two-star case, the primary (i.e more luminous) component is a B-type star of surface temperature $T_{\rm eff,B} \simeq 15\,000\,{\rm K}$ and (magnified) luminosity $\log(\mu L_{\rm B}/{\rm L}_\odot) \simeq 9.43$ with an F-type star companion of $T_{\rm eff,F} \simeq 6\,250\,{\rm K}$ and $\log(\mu L_{\rm F}/{\rm L}_\odot) \simeq 9.04$. Under reasonable assumptions on the magnification, both components correspond to high-mass stars (initial masses $\gtrsim 10\,{\rm M}_\odot$ for $\mu < 50\,000$), with $\mu \gtrsim 1\,300$ required to bring the more luminous star down to an initial mass $\lesssim 100\,{\rm M}_\odot$. This combination of stars would be unexpected for several reasons. Unless $\mu > 1\,000 - 3\,000$, both stars violate the empirical Humphreys–Davidson luminosity limit (caused by envelope-stripping due to stellar winds Humphreys & Davidson 1979). Moreover, the recent stellar evolutionary models for high-mass stars by Szécsi et al. (2022) suggest that the evolutionary states corresponding to the best-fitting surface temperature would be extremely brief ($\lesssim 10^5$ yr), except at very specific masses and metallicities. Under the assumption that the two stars have similar magnifications, the ratio of bolometric luminosities ($L_{\rm B}/L_{\rm F} \approx 2.4$) also causes a potential age problem. While our constraints on the source size in no way require the two stars to be part of the same

binary system, they are still likely to be young members of the same star cluster, and hence have similar ages. In the context of single-star evolution, stars with higher luminosity and initial mass typically evolve to low-$T_{\rm eff}$ states ahead of their lower-L and less massive counterparts, whereas the opposite seems to be the case here. While blue loops along the evolutionary track of the more massive star could potentially provide an explanation, this requires finely tuned ages given the large $L_{\rm B}/L_{\rm F}$-ratio. This problem could also be resolved in a scenario where the inferred luminosity ratio is strongly affected by dust attenuation along the line of sight, either from circumstellar or interstellar dust. In a situation where the light from the lower-$T_{\rm eff}$ star is experiencing significantly more dust attenuation than the higher-$T_{\rm eff}$ star, the intrinsic $L_{\rm B}/L_{\rm F}$-ratio would be lower than that inferred from our current fit. We have also searched through the suite of binary models from the *Binary Population And Spectral Synthesis* (BPASS; v2.2) results (Stanway & Eldridge 2018). The only matches with the effective temperatures and luminosity ratios matching our two-star fit are low-mass stars of a few M$_\odot$. These would require even more extreme magnifications though due to the relatively low luminosities of low-mass stars. This suggests that our object is unlikely to be part of a co-evolving binary. One more possibility that needs mentioning is a redder star accompanied by a stellar-mass black hole accretion disc as suggested in Windhorst et al. (2018), although that would have much higher temperatures and therefore a bluer spectrum than our object.

In the single-star scenario, we are also looking at a B-type star of $T_{\rm eff} \simeq 15\,000\,{\rm K}$ which is however somewhat brighter ($\log(\mu L/{\rm L}_\odot) \simeq 10.13$) and considerably reddened by dust to $A_V \simeq 0.82$ magnitudes. In this case, a magnification of $\mu \gtrsim 7\,000$ would be required to bring the star below $\lesssim 100\,{\rm M}_\odot$, based on the evolutionary tracks of Szécsi et al. (2022). In both cases the fit is driven by a $T_{\rm eff} \simeq 15\,000\,{\rm K}$ B-type super-giant and the companion or dust attenuation are reducing the strength of the Balmer-break and flattening the continuum at longer wavelengths to match the spectrum. The surface temperature is somewhat higher than inferred from the photometry in Meena et al. (2023b) ($T_{\rm eff} \simeq 10\,500\,{\rm K}$). The present data do not enable us to clearly distinguish between these two solutions as both scenarios provide a good fit to the spectrum ($\chi^2 \simeq 1$). The single-star solution is easier to explain using current stellar evolutionary models however.

4.2 Stellar population modelling

In order to explore the possibility of our source being a star-cluster instead of one or two single lensed stars, we perform an additional spectral fit with the BEAGLE tool (Chevallard & Charlot [2016](#)). We use the latest version of the Bruzual & Charlot ([2003](#)) stellar population models combined with nebular emission models by Gutkin, Charlot & Bruzual ([2016](#)), a Charlot & Fall ([2000](#)) dust attenuation law and the Inoue et al. ([2014](#)) intergalactic medium (IGM) attenuation models. The star cluster is parametrized as a SSP with four free parameters: the (magnified) stellar mass ($\log(\mu M_\star/M_\odot) \in [4, 10]$), age ($\log(t_{\text{age}}/\text{yr}) \in [6, t_{\text{Universe}}]$), dust attenuation ($\hat{\tau}_V \in [0, 0.1]$), and metallicity ($\log(Z/Z_\odot) \in [-3, 0.4]$). The result of this fit is shown in the right-hand panel of Fig. [3](#).

4.3 A star or a star cluster? Insight from lensing

All three options shown in Fig. [3](#), namely a single star + dust, two stars, or a star cluster, yield similarly good fits to the spectral data, rendering all options viable. However, we can use constraints from lensing symmetry, magnification, and possible flux variability, to obtain some more insight regarding the nature of the source. Indeed, given that the source lies very close to the critical curves where the magnification gets extremely high, the latter is very difficult to measure. We start by noting that based on the SL model by Meena et al. ([2023b](#)), the total magnification at the position of star-1, which lies ∼0.04″ from the critical curves of the model, is $\mu \sim 600$, whereas the tangential magnification is $\mu_t \sim 500$. Given that the lensed source remains point-like, we can adopt the point-spread-function (PSF) of 0.04″, which translates into an upper limit of $r \lesssim 0.3$ pc on the size of the source. In fact, since the position of the critical line can be constrained independently from the SL model by symmetry considerations (Fig. [1](#); see also fig. 3 in Meena et al. [2023b](#)), we can also infer a more model-independent estimate. Star-1 lies about 0.1″ from the deduced symmetry point, which results in an upper-limit of $r \lesssim 0.5$ pc, corresponding to a magnification of $\mu \sim 250$.

Note that if this object were a star cluster, then from the stellar population fit in Section [4.2](#) it would have a magnified stellar mass of $\log(\mu M_\star/M_\odot) = 8.42^{+0.03}_{-0.02}$. Combining this stellar mass with the magnification and size estimates, we obtain that the intrinsic (i.e. delensed) projected stellar mass density would be $\Sigma_\star \simeq 2.1 \times 10^6 \, M_\odot/\text{pc}^2$. This is more than an order of magnitude higher than the highest densities observed in globular clusters (e.g. Norris et al. [2014](#)) or young massive star clusters known to date, both at low and high redshifts (e.g. Brown & Gnedin [2021](#); Vanzella et al. [2023](#)), and two orders of magnitude higher than the highest densities found in high-resolution simulations (e.g. He, Ricotti & Geen [2019](#); Garcia et al. [2023](#)), therefore making the star-cluster option more challenging.

The star-cluster option, alternatively, is consistent with the lack of flux variability in the F200W-band which repeated in both epochs: since star clusters are larger and much more complex compared to stars, only very weak fluctuations are expected (e.g. Dai [2021](#)). Nevertheless, stars in the corrugated network of micro-caustics which forms around the macro-caustic are also expected to show only mild fluctuations (e.g. Welch et al. [2022a](#)). For dense networks of micro-caustics, the time variation can be very rapid but small in amplitude and thus the source may appear constant for a relatively long period of time. The mere two epochs in one band are likely insufficient for drawing a conclusion based on variability at this stage.

There is another challenge to the star-cluster possibility: the source lacks a counter image on the other side of the critical curves (or

the symmetry axis). For the source to be a star-cluster and not show a counter image, one would have to invoke a milli-lens to create a local area of demagnification and thus 'hide' the counter image. While plausible, this would require some fine-tuning, which complicates the interpretation. In that regard it is worth mentioning another possibility: in the case of 'wave dark matter', the network of caustics is pervasive and thus small sources can be strongly magnified without new counter images appearing (Amruth et al. [2023](#)). In this framework the source could in principle be a star cluster, without a need to invoke additional perturbers.

The most plausible solution may simply be, as originally proposed, a star very near the macro-caustic, that is, in the corrugated network of micro-caustics, in which case no counter images are necessarily expected on the other side of the macro critical curves. As is evident in Fig. [1](#), the star lies between the model's critical curve and the model-independent symmetry line. The true position of the critical curve lies most likely somewhere between these two lines, meaning that star-1 is $\lesssim 0.1″$ from it. For comparison, the size of the corrugated network, which depends on the micro-lens surface density and its mass function, as well as on the underlying lensing quantities (such as the lens-mapping Jacobian's eigenvalues; Venumadhav et al. [2017](#)), is of the same order – assuming that about 1 per cent of the surface mass density consists of microlenses. Note also that in order for an object to remain a point-source in such a scenario, that is, to appear smaller than the given PSF of 0.04″, its radius cannot exceed $r \lesssim 0.01$ pc, corresponding to a magnification of $\mu \sim \mathcal{O}(10^4)$ (see formulae in Venumadhav et al. [2017](#); Meena et al. [2023b](#)).

Based on the earlier considerations we therefore conclude that the scenario of a young globular cluster is somewhat less likely, even though it cannot be ruled out with the present data either and remains a viable option. Distinguishing better the two scenarios would require a higher SNR which would allow us to measure absorption lines, as well as additional visits to examine further the flux variability.

5 CONCLUSION

We have presented a JWST/NIRSpec prism spectrum of the extremely lensed star candidate MACS0647-star-1, detected previously in JWST/NIRCam imaging of the SL cluster MACS J0647.7+7015. The slit covers also a portion of the host arc which shows two prominent emission lines, identified as the unresolved [O III]λλ4959, 5007 Å-doublet and the Hα line. These allow us to precisely measure the spectroscopic redshift at $z_{\text{spec}} = 4.758 \pm 0.004$. We subtract the contribution of the host galaxy to obtain a clean spectrum of the star, which shows clear Lyman- and Balmer-breaks at the same redshift but – given the SNR – lacks significant absorption (or emission) features. Spectral fits considering both a single and a two-star solution find this object to most likely be a B-type super-giant star of surface temperature $T_{\text{eff}} \simeq 15\,000$ K with either an F-type companion of $T_{\text{eff}} \simeq 6\,250$ K or significant dust attenuation of $A_V \simeq 0.82$ originating from the star's surroundings. We also explore the possibility of the object being a globular cluster progenitor and fit it with an SSP template which results in a (magnified) stellar mass estimate of $\mu M_\star \simeq 10^{8.4} \, M_\odot$. Given that this would result in an extremely high-stellar mass density when combined with the lensing constraints on the radius of our object ($r \lesssim 0.5$ pc, for $\mu \gtrsim 250$) and would produce a counter image which we do not detect, this solution is somewhat disfavoured compared to the star solutions.

By delivering JWST's first spectrum of an extremely magnified star candidate at nearly $z \sim 5$, this work clearly showcases the phenomenal potential of JWST to probe individual stars across the history of the Universe with the aid of gravitational lensing. In order

to explore the properties of these sources in detail and clearly distinguish between a single star and a star-cluster, various visits are needed to examine variability, as well as deeper observations to follow-up on the tentative absorption lines – and at potentially higher spectral resolutions than provided by the NIRSpec prism mode. These might be achieved, for example, with the higher-resolution gratings on NIRSpec (optimally with spectral resolutions of $R \sim 1\,000$), but would require longer exposure times and, preferably, brighter stars.

Some prominent lensed stars have also already been targeted spectroscopically from the ground at lower redshifts (e.g. *Godzilla*). Obtaining spectra of lensed stars could thus represent a compelling science case also for upcoming extremely large telescopes, combining unprecedented spatial resolution and the collecting power of 30–40 m class mirrors with significantly higher spectral resolution ($R \gtrsim 10\,000$ class) spectrographs.

ACKNOWLEDGEMENTS

This research made use of `Astropy`,[7] a community-developed core Python package for Astronomy (Astropy Collaboration et al. 2013; Price-Whelan et al. 2018) as well as the packages `NUMPY` (van der Walt, Colbert & Varoquaux 2011), `SCIPY` (Virtanen et al. 2020), `MATPLOTLIB` (Hunter 2007), and the `MAAT` Astronomy and Astrophysics tools for `MATLAB` (Ofek 2014).

DATA AVAILABILITY

REFERENCES

Amruth A. et al., 2023, Nature Astron., 7, 736
Astropy Collaboration et al., 2013, A&A, 558, 33
Böker T. et al., 2023, PASP, 135, 038001
Brammer G., Strait V., Matharu J., Momcheva I., 2022, grizli, https://doi.org/10.5281/zenodo.6672538
Brown G., Gnedin O. Y., 2021, MNRAS, 508, 5935
Bruzual G., Charlot S., 2003, MNRAS, 344, 1000
Calzetti D., Armus L., Bohlin R. C., Kinney A. L., Koornneef J., Storchi-Bergmann T., 2000, ApJ, 533, L682
Charlot S., Fall S. M., 2000, ApJ, 539, L718
Chen W. et al., 2019, ApJ, 881, L8
Chen W. et al., 2022, ApJ, 940, L54
Chevallard J., Charlot S., 2016, MNRAS, 462, 1415
Coe D. et al., 2013, ApJ, 762, L32
Dai L., 2021, MNRAS, 501, 5538
Diego J. M. et al., 2018, ApJ, 857, L25
Diego J. M., Pascale M., Kavanagh B. J., Kelly P., Dai L., Frye B., Broadhurst T., 2022, A&A, 665, 134
Diego J. M. et al., 2023a, preprint (arXiv:2304.09222)
Diego J. M. et al., 2023b, preprint (arXiv:2307.10363)
Diego J. M. et al., 2023c, A&A, 672, 3
Domínguez A. et al., 2013, ApJ, 763, L145
Earl N. et al., 2023, astropy/specutils: v1.10.0,, https://doi.org/10.5281/zenodo.7803739
Ebeling H., Barrett E., Donovan D., Ma C.-J., Edge A. C., van Speybroeck L., 2007, ApJ, 661, L33
Ferruit P. et al., 2022, A&A, 661, 81
Foreman-Mackey D., Hogg D. W., Lang D., Goodman J., 2013, PASP, 125, 306
Garcia F. A. B., Ricotti M., Sugimura K., Park J., 2023, MNRAS, 522, 2495
Gardner J. P. et al., 2023, PASP, 135, 068001
Gutkin J., Charlot S., Bruzual G., 2016, MNRAS, 462, 1757
He C.-C., Ricotti M., Geen S., 2019, MNRAS, 489, 1880
Hsiao T. Y.-Y. et al., 2023a, preprint (arXiv:2305.03042)
Hsiao T. Y.-Y. et al., 2023b, ApJ, 949, L34
Humphreys R. M., Davidson K., 1979, ApJ, 232, L409
Hunter J. D., 2007, Comput. Sci Eng., 9, 90
Inoue A. K., Shimizu I., Iwata I., Tanaka M., 2014, MNRAS, 442, 1805
Jakobsen P. et al., 2022, A&A, 661, 80
Jiménez-Teja Y., Dupke R., 2016, ApJ, 820, L49
Jiménez-Vicente J., Mediavilla E., 2022, ApJ, 941, L80
Kaurov A. A., Dai L., Venumadhav T., Miralda-Escudé J., Frye B., 2019, ApJ, 880, L58
Kelly P. L. et al., 2018, Nature Astron., 2, 334
Kelly P. L. et al., 2022, preprint (arXiv:2211.02670)
Lejeune T., Cuisinier F., Buser R., 1997, A&AS, 125, 229

Li A., Liang S. L., Kann D. A., Wei D. M., Klose S., Wang Y. J., 2008, ApJ, 685, L1046

Meena A. K. et al., 2023a, MNRAS, 521, 5224

Meena A. K. et al., 2023b, ApJ, 944, L6

Miralda-Escude J., 1991, ApJ, 379, L94

Norris M. A. et al., 2014, MNRAS, 443, 1151

Ofek E. O., 2014, MAAT: MATLAB Astronomy and Astrophysics Toolbox, Astrophysics Source Code Library, record ascl:1407.005

Oguri M., Diego J. M., Kaiser N., Kelly P. L., Broadhurst T., 2018, Phys. Rev. D, 97, 023518

Oke J. B., Gunn J. E., 1983, ApJ, 266, L713

Postman M. et al., 2012, ApJS, 199, 25

Price-Whelan A. M. et al., 2018, AJ, 156, 123

Rieke M. J. et al., 2023, PASP, 135, 028001

Stanway E. R., Eldridge J. J., 2018, MNRAS, 479, 75

Szécsi D., Agrawal P., Wünsch R., Langer N., 2022, A&A, 658, 125

van der Walt S., Colbert S. C., Varoquaux G., 2011, Comput. Sci Eng., 13, 22

Vanzella E. et al., 2020, MNRAS, 499, 67

Vanzella E. et al., 2023, ApJ, 945, L53

Venumadhav T., Dai L., Miralda-Escudé J., 2017, ApJ, 850, L49

Virtanen P. et al., 2020, Nature Methods, 17, 261

Welch B. et al., 2022a, Nature, 603, 815

Welch B. et al., 2022b, ApJ, 940, L1

Windhorst R. A. et al., 2018, ApJS, 234, 41

Zitrin A., Broadhurst T., Barkana R., Rephaeli Y., Benítez N., 2011, MNRAS, 410, 1939

Zitrin A. et al., 2015, ApJ, 801, L44

[1]*Physics Department, Ben-Gurion University of the Negev, P.O. Box 653, Be'er-Sheva 84105, Israel*

[2]*Observational Astrophysics, Department of Physics and Astronomy, Uppsala University, Box 516, SE-751 20 Uppsala, Sweden*

[3]*Cosmic Dawn Center (DAWN), Niels Bohr Institute, University of Copenhagen, Jagtvej 128, København N, DK-2200, Denmark*

[4]*Space Telescope Science Institute (STScI), 3700 San Martin Drive, Baltimore, MD 21218, USA*

[5]*Association of Universities for Research in Astronomy (AURA) for the European Space Agency (ESA), STScI, Baltimore, MD 21218, USA*

[6]*Department of Physics and Astronomy, Center for Astrophysical Sciences, The Johns Hopkins University, 3400 North Charles Street Baltimore, MD 21218, USA*

[7]*Instituto de Física de Cantabria (CSIC-UC), Avenida de los Castros s/n. E-39005 Santander, Spain*

[8]*Department of Physics, University of Auckland, Private Bag 92019, Auckland, New Zealand*

[9]*Instituto de Astrofísica de Andalucía, Glorieta de la Astronomía s/n, E-18008 Granada, Spain*

[10]*Observatório Nacional - MCTI (ON), Rua Gal. José Cristino 77, São Cristóvão, 20921-400, Rio de Janeiro, Brazil*

[11]*Kapteyn Astronomical Institute, University of Groningen, P.O. Box 800, NL-9700AV Groningen, the Netherlands*

[12]*Department of Astronomy, University of Maryland, College Park, MD 20742, USA*

[13]*Observational Cosmology Lab, NASA Goddard Space Flight Center, Greenbelt, MD 20771, USA*

[14]*School of Earth and Space Exploration, Arizona State University, Tempe, AZ 85287-1404, USA*

[15]*Department of Liberal Arts and Sciences, Berklee College of Music, 7 Haviland Street, Boston, MA 02215, USA*

[16]*Center for Astrophysics, Harvard & Smithsonian, 60 Garden Street, Cambridge, MA 02138, USA*

[17]*European Space Agency (ESA), European Space Astronomy Centre (ESAC), Camino Bajo del Castillo s/n, E-28692 Villanueva de la Cañada, Madrid, Spain*

[18]*Department of Theoretical Physics, University of the Basque Country (UPV/EHU), Bilbao 48080, Spain*

[19]*Donostia International Physics Center (DIPC), Donostia 20018, Spain*

[20]*Ikerbasque (Basque Foundation for Science), Bilbao 48009, Spain*

[21]*School of Physics and Astronomy, University of Minnesota, 116 Church Street SE, Minneapolis, MN 55455, USA*

[22]*Jodrell Bank Centre for Astrophysics, University of Manchester, Oxford Road, Manchester M13 9PL, UK*

[23]*Department of Astronomy/Steward Observatory, University of Arizona, 933 North Cherry Avenue, Tucson, AZ 85721, USA*

[24]*Department of Astronomy, The University of Texas at Austin, Austin, TX 78712, USA*

[25]*Institute for Computational Cosmology, Durham University, South Road, Durham DH1 3LE, UK*

[26]*Centre for Extragalactic Astronomy, Durham University, South Road, Durham DH1 3LE, UK*

[27]*Racah Institute of Physics, The Hebrew University, Jerusalem 91904, Israel*

[28]*Center for Frontier Science, Chiba University, 1-33 Yayoi-cho, Inage-ku, Chiba 263-8522, Japan*

[29]*Department of Physics, Graduate School of Science, Chiba University, 1-33 Yayoi-Cho, Inage-Ku, Chiba 263-8522, Japan*

[30]*INAF – OAS, Osservatorio di Astrofisica e Scienza dello Spazio di Bologna, via Gobetti 93/3, I-40129 Bologna, Italy*

[31]*Astronomy Centre, University of Sussex, Falmer, Brighton BN1 9QH, UK*

[32]*Institute of Space Sciences and Astronomy, University of Malta, 31 Msida, MSD 2080, Malta*

This paper has been typeset from a TEX/LATEX file prepared by the author.